J. Astrophys. Astr. (2021)42:60
https://doi.org/10.1007/s12036-021-09757-9

UBVI CCD photometry of Berkeley 55 open cluster

İNCI AKKAYA ORALHAN

Department of Astronomy and Space Sciences, Science Faculty, Erciyes University, 38039 Kayseri, Turkey.
E-mail: iakkaya@erciyes.edu.tr

MS received 26 January 2021; accepted 2 March 2021

Abstract. Fundamental astrophysical parameters have been derived for Berkeley 55 (Be 55) open cluster based on the UBVI charge-coupled device (CCD) photometric data observed using a AZT-22 1.5 m telescope at Maidanak Astronomical Observatory (MAO) in Uzbekistan. The mean reddening is obtained as $E(B-V) = 1.77 \pm 0.10$ mag from early-type members. The zero-age main sequence fitting in the $Q_{V\lambda} - Q'$ diagrams indicates the distance modulus, $(V_0 - M_V) = 12.4 \pm 0.20$ mag ($d = 3.02 \pm 0.28$ kpc). This photometric distance is consistent with the distances of Gaia EDR3 ($d = 3.09 \pm 0.16$ kpc) and period–luminosity relation ($d = 2.78 \pm 0.32$ kpc) of its Cepheid *S*5 within the uncertainties. This distance also locates the cluster near the Perseus spiral arm. The Geneva isochrone fittings to the Hertzsprung–Russell diagram and observational colour–magnitude diagrams derive turn-off age, 85 ± 13 Myr, by taking care of five red supergiants/bright giants. The possible inconsistencies in the locations of the bright giants with the rotating/non-rotating isochrones may be due to both the age spread of stars in young open clusters and the diversity in rotational velocities.

Keyword. Open clusters and associations—individual Berkeley 55-stars—early-type stars evolution—late-type supergiants.

1. Introduction

Berkeley 55 (Be 55) was studied by Negueruela & Marco (2012), Lohr *et al.* (2018), and Alonso-Santiago *et al.* (2020). Negueruela & Marco (2012) identified populations of B-type stars, one F-type star, four late-type red supergiants (RSGs)/red bright giants (RBGs), and two blue stragglers (BSs). Their spectroscopic and photometric analyses indicated an age of 50 ± 10 Myr and a distance of $d \approx 4$ kpc. Its member *S*5 was identified by Lohr *et al.* (2018) as a Type I Cepheid with a pulsation period of 5.85 days. Spectral types, effective temperatures, and radial velocities of these bright giants have been obtained by Alonso-Santiago *et al.* (2020) from the medium resolution spectroscopic observations of a 4.2 m William Herschel Telescope at La Palma. They updated the distance and age of Be 55 as 3.24 ± 0.22 kpc and 63 ± 15 Myr, respectively, from PARSEC isochrones (Bressan *et al.* 2012). Be 55 OCs were also studied by Maciejewski & Niedzielski (2007), Tadross (2008), Bukowiecki *et al.* (2011), and Molina *et al.* (2018) (see Table 1).

As emphasized by Alonso-Santiago *et al.* (2020), Cepheids in young OCs, which lie on the blue loop as a pulsating variable, have great importance for distance estimation. For their distances, there are useful period–luminosity relations (PLRs) in the literature (Benedict 2007; Anderson *et al.* 2013; Lazovik & Rastorguev 2020). Some young OCs with Cepheids as examples are as follows: van den Bergh–Hagen (Marco *et al.* 2014), Be 51 (Negueruela *et al.* 2018), and NGC 6649 and NGC 6664 (Alonso-Santiago *et al.* 2020).

Young OCs are generally heavily obscured. For their reddenings, *Q* technique from their early-type stars is used (Sung *et al.* 2013). For their bright evolved stars, the intrinsic colours of Fernie (1963) and Fitzgerald (1970) for UBV and Koornneef (1983) for JHK_s are utilised.

In this paper, a new Maidanak UBVI charge-coupled device (CCD) photometry of Be 55 OC is

Published online: 29 June 2021

Table 1. Comparison with the literature for Be 55.

$E(B-V)$ (mag)	$V_0 - M_V$ (mag)	d (kpc)	Z	Log age	Age (Myr)	Isochrone	Photometry	References
1.77 ± 0.10	12.40 ± 0.20	3.02 ± 0.28	0.014	7.93 ± 0.06	85 ± 13	Ekström *et al.* (2012)	CCD UBVI	This paper
1.74 ± 0.07	11.71 ± 0.30	2.20 ± 0.30		7.80	63 ± 12	PLR of S5 Cepheid	CCD VR	Lohr *et al.* (2018)
1.85 ± 0.16	13.0 ± 0.30	3.98 ± 0.55	Solar	7.70	50 ± 10	Marigo *et al.* (2008)	CCD UBV	Negueruela & Marco (2012)
1.81 ± 0.15	12.55 ± 0.15	3.24 ± 0.22	Solar	7.80 ± 0.10	63 ± 15	Ekström *et al.* (2012)	CCD UBV	Alonso-Santiago *et al.* (2020)
1.75	12.40	3.02	Solar	7.50–8.50	30–100	Bressan *et al.* (2012)	ugr	Molina *et al.* (2018)
1.74 ± 0.10	10.42	1.21 ± 0.31	Solar	8.50	315	Bertelli *et al.* (1994)	CCD BV	Maciejewski & Niedielski (2007)
1.50		1.44 ± 0.07	Solar	8.48	300	Bonatto *et al.* (2004)	2MASS-JHK$_s$	Tadross (2008)
1.15	12.23	1.70 ± 0.13	0.019	8.95	891	Girardi *et al.* (2002)	2MASS-JK$_s$	Bukowiecki *et al.* (2011)
$1.55(A_V = 4.8)$	12.20	2.75	0.015	8.30	200	Bressan *et al.* (2012)	Gaia DR2	Cantat-Gaudin *et al.* (2018, 2020)

presented, and analysed by utilising Gaia EDR3 astrometric/photometric data (Brown 2020; Lindegren *et al.* 2020). The issues mentioned above have been studied. As emphasized by Lindegren *et al.* (2020), compared with Gaia DR2 (Brown *et al.* 2018; Lindegren *et al.* 2018), the average improvement on the uncertainties of parallax/proper motion data of Gaia EDR3 is almost a factor of 0.8 for the parallaxes, and 0.5 for the proper motions.

This paper is organized as follows: Section 2 describes the observation and data reduction. The radius, membership selection, determination of the reddening, and distance modulus/distance are presented in Section 3. Be 55's age plus kinematics/orbital parameters of its bright giants are given in Sections 4 and 5. A discussion and conclusion is presented in Section 6.

2. Observation and data reduction

The observation in the Johnson-Cousins' UBVI system of Be 55 was performed using an AZT-22 1.5 m (f/7.74) Ritchey-Chretien telescope at the MAO in Uzbekistan, during a high-quality photometric night, on 9 August 2005. Images were taken using an SITe 2k CCD detector, which has 2000×800 pixels, a gain of $1.16e^-$/ADU and a readout noise of $5.3e^-$. The combination of the telescope and the detector ensures an unvignetted field of view of $8.85' \times 3.55'$. The standard magnitude for a given filter λ is obtained using the following relation:

$$M_\lambda = m_\lambda - [k_{1\lambda} - k_{2\lambda}C)]X + \eta_\lambda C + \zeta_\lambda, \quad (1)$$

where m_λ, $k_{1\lambda}$, $k_{2\lambda}$, C, and X are the observed instrumental magnitude, primary/secondary extinction coefficients, colour index, and air mass, respectively. M_λ, η_λ, and ζ_λ are standard magnitude, transformation coefficient, and photometric zero point, respectively. The other details of data reduction can be found in Lim *et al.* (2009). The South African Astronomical Observatory (SAAO) standard stars in Menzies *et al.* (1991) and Kilkenny *et al.* (1998) were used to derive atmospheric extinction and transformation coefficients. Pre-processing was performed using the IRAF/CCDRED package and an aperture of $10''$ was used for the standard star photometry. Exposure time (s), FWHM-seeing ($''$), extinction coefficients, and zero points for UBVI filters are given in Table 2. Here, FWHM-seeing means the seeing, which is estimated from FWHM of the point-like stars on the images. The

Table 2. UBVI filters, exposure time, full width at half maximum (FWHM)-seeing, the primary/secondary extinction coefficients ($k_{1\lambda}$, $k_{2\lambda}$), and the photometric zero-point (ζ_λ).

Filter	Colour	Exposure time (s)	FWHM-seeing ($''$)	$k_{1\lambda}$	$k_{2\lambda}$	ζ_λ
U	U–B	600	1.22	0.423 ± 0.022	0.023	21.560 ± 0.011
B	B–V	20, 600	1.99	0.324 ± 0.010	0.026	23.261 ± 0.006
V	B–V	10, 300	0.88	0.231 ± 0.009	–	23.396 ± 0.001
I	V–I	10, 120	0.74	0.139 ± 0.010	–	23.017 ± 0.009

Table 3. Photometric data of Be 55.

α_{2000} (h m s)	δ_{2000} ($^\circ\,'\,''$)	V-mag	$(U-B)$	$(B-V)$	$(V-I)$	eV	$e(V-I)$	$e(B-V)$	$e(U-B)$
21 16 51.27	51 46 07.3	15.186	0.524	1.562	2.130	0.003	0.011	0.004	0.009
21 17 2.30	51 46 58.1	14.666	0.581	1.543	2.017	0.001	0.001	0.001	0.006
21 17 1.72	51 46 49.1	15.771	0.721	1.532	2.021	0.001	0.005	0.004	0.016

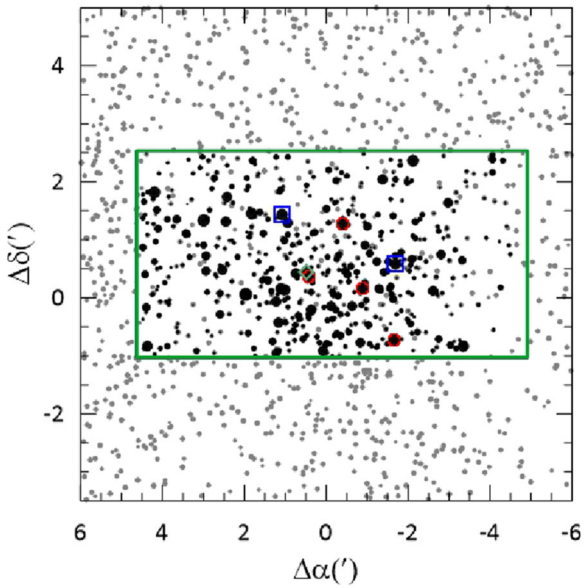

Figure 1. Star chart of Be 55 based on Gaia EDR3 data (grey dots) and Maidanak 2k data (black dots). The position of the stars is relative to their mean equatorial coordinates. Green rectangular shows the field of view of the Maidanak detector. Five RSGs/RBGs and two BSs are also indicated (see Figure 6 for the symbols).

photometric data of 357 stars are listed in Table 3 for sample data.

The Be 55′ star chart is shown in Figure 1. Its mean central equatorial (J2000) and galactic coordinates are as follows: RA = $21^{\rm h}$ $16^{\rm m}$ $58^{\rm s}.01$, Dec = $+51^\circ 45' 32''.04$; $\ell = 93^\circ.027$, $b = 1^\circ.798$, respectively.

Table 4. Mean photometric errors of $\langle V\rangle$ mag, $\langle(V-I)\rangle$, $\langle(B-V)\rangle$ and $\langle(U-B)\rangle$ against V-mag.

V	$\langle\sigma_V\rangle$	$\langle\sigma_{V-I}\rangle$	$\langle\sigma_{B-V}\rangle$	$\langle\sigma_{U-B}\rangle$
13–14	0.003	0.013	0.008	0.005
14–15	0.005	0.020	0.007	0.016
15–16	0.008	0.007	0.007	0.017
16–17	0.005	0.007	0.009	0.032
17–18	0.006	0.009	0.010	0.065
18–19	0.012	0.016	0.023	0.129
19–20	0.016	0.021	0.053	–
20–21	0.050	0.052	0.123	–
21–22	0.090	0.095	0.156	–
22–23	0.150	0.157	–	–

The mean photometric errors of V mag, the colour indices $(V-I)$, $(B-V)$ and $(U-B)$ against V-mag for Be 55 are presented in Table 4. The photometry for Be 55 is compared with the UBV CCD photometry of Negueruela & Marco (2012). For 26 common stars, the differences of ΔV and $\Delta(B-V)$ against $(B-V)$, and the difference of $\Delta(U-B)$ against $(U-B)$ are shown in Figure 2. When the large deviant data of the evolved stars are excluded from the calculation, the mean differences together with dispersions of V and $(B-V)$ are $\Delta V = +0.036 \pm 0.027$ mag and $\Delta(B-V) = +0.003 \pm 0.012$, respectively. The difference, $\Delta(U-B)$ is $+0.082 \pm 0.064$, which is systematically bluer than Negueruela & Marco (2012). For the interval of $14 < V < 18$ mag, the V magnitudes of Negueruela & Marco (2012) seem to be slightly fainter. For $14 < V < 18$ mag, the B–V values of this paper are

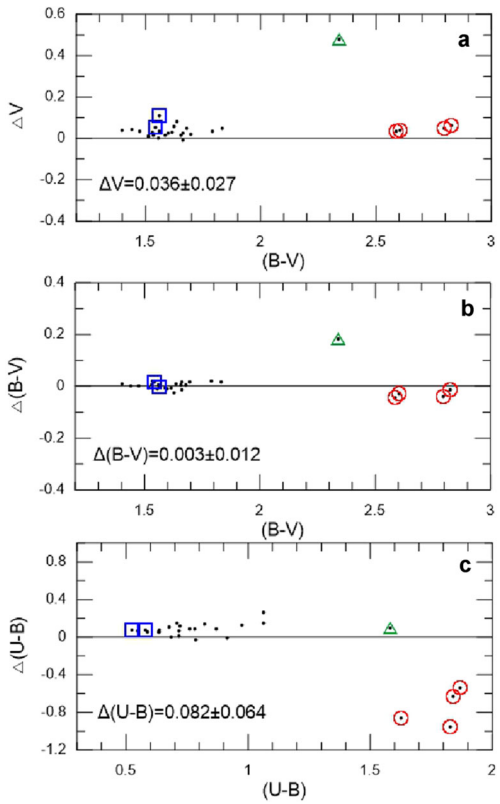

Figure 2. Differences of V mag, $(B-V)$ and $(U-B)$ as a function of $(B-V)$ and $(U-B)$. Δ means this paper Negueruela & Marco (2012). Five RSGs/RBGs are plotted for just presentation (for the symbols, see Figure 6).

in good agreement with Negueruela & Marco (2012), except for bright giants. In panel (c) there appears a discrepancy between -0.4 and -1.0 in U–B of four RBGs/RSGs between Negueruela, Marco and Maidanak observations. For Cepheid S5 (red diamond), the discrepancy is about 0.50 mag in ΔV and 0.2 mag in $\Delta(B-V)$ from panels (a) and (b). The reason for the large colour difference for four late-type supergiants with very red colours between $(U-B)$ of the present photometry and Negueruela & Marco (2012) is due to the so-called red leak in the used U filter. Therefore, their U-magnitudes of the present photometry are brighter than Negueruela & Marco (2012). However, there is no red leak effect in the used U filter, as is shown in Table 3 of the transformation coefficients of Lim *et al.* (2009).

3. Fundamental parameters of Be 55

3.1 *Radius of Be 55*

For the size of Be 55, its stellar radial density profile (RDP) (Figure 3) is constructed from the Gaia EDR3

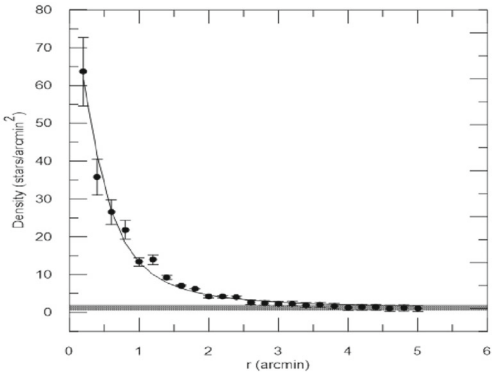

Figure 3. RDP of Be 55. The curved line shows the fitting of King (1966). The vertical bars denote the Poisson errors.

photometric/astrometric data for the field and cluster members within $15'.0$, down to $G = 20$ mag. Its RDP has been constructed by counting stars in concentric rings of increasing width with distance to its centre. The number and width of rings were optimised so that the resulting RDP had an adequate spatial resolution with moderate 1σ Poisson errors (Bonatto & Bica 2007). The solid curve (Figure 3) denotes the fitted King's profile (King 1966). The two-parameter function $\sigma(R) = \sigma_{\rm bg} + \sigma_0/(1 + (R/R_{\rm c})^2)$ is adopted. Here, $\sigma_{\rm bg}$ is the residual background density, σ_0 is the central density of stars, and $R_{\rm core}$ is the core radius. The horizontal grey bar shows the stellar background level measured in the comparison field. From Figure 3, the core and cluster radii have been determined as $(R_{\rm core}, R_{\rm RDP}) = (0'.45, 2'.5)$. The cluster radius is compatible with $2'.5$ of Molina *et al.* (2018) and $2'.2$ of Sampedro *et al.* (2017). The $R_{\rm core}$ value of this paper is $<1'.32$ of Bukowiecki *et al.* (2011), $0'.90$ of Kharchenko *et al.* (2013), and $1'.28$ of Alonso-Santiago *et al.* (2020), respectively.

3.2 *Membership selection*

In Akkaya Oralhan *et al.* (2019, 2020), UBVI photometric data of Be 55 have been combined with Gaia EDR3 proper motion and parallax data (Brown 2020; Lindegren *et al.* 2020) to classify the likely cluster members. On the (μ_α, μ_δ) plane (Figure 4), 305 stars (filled dots) within $R_{\rm RDP} = 2'.5$ are shown. The grey dots represent the field background/foreground stars with a region centred around 15 arcmin. The fitted radius (red circle) by eye is determined as 0.5 mas yr^{-1} by utilising the histograms (shown with red lines) attached to the μ_α *vs.* μ_δ plot. One hundred and nine probable members in the red circle are used

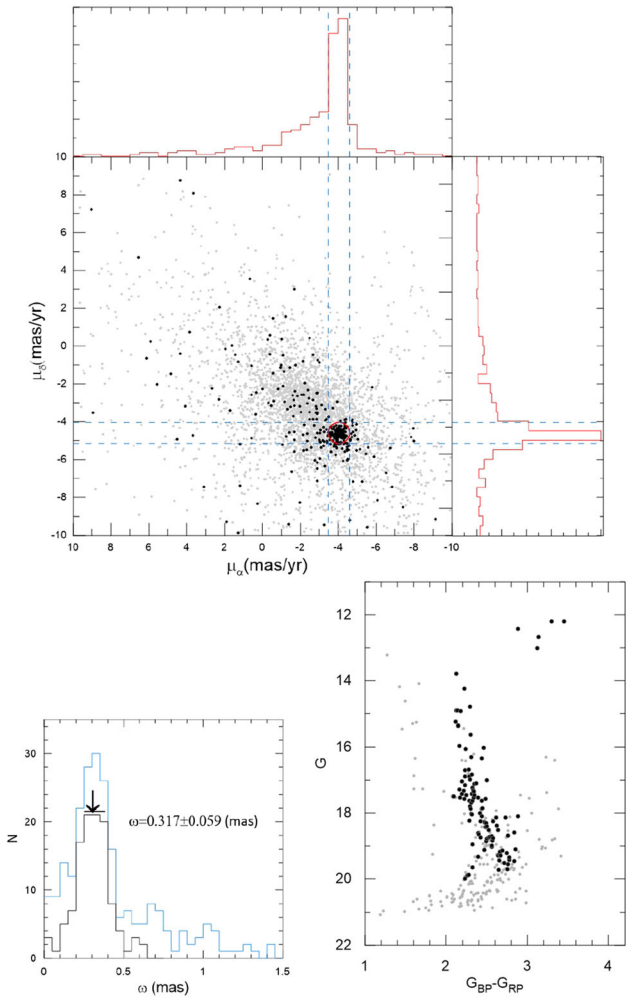

Figure 4. The μ_α *vs.* μ_δ for 305 stars of Be 55 (filled dots). The field stars inside 15 arcmin are shown with small grey dots. There are probable 109 members in the red circle as the fitted proper motion circle (0.5 mas yr^{-1}). Gaia EDR3 parallax (ϖ) histogram (left panel) for 305 (blue) and 109 members (red). On $(G, G_{\rm BP} - G_{\rm RP})$, single stellar cluster sequences of the probable members are clearly visible.

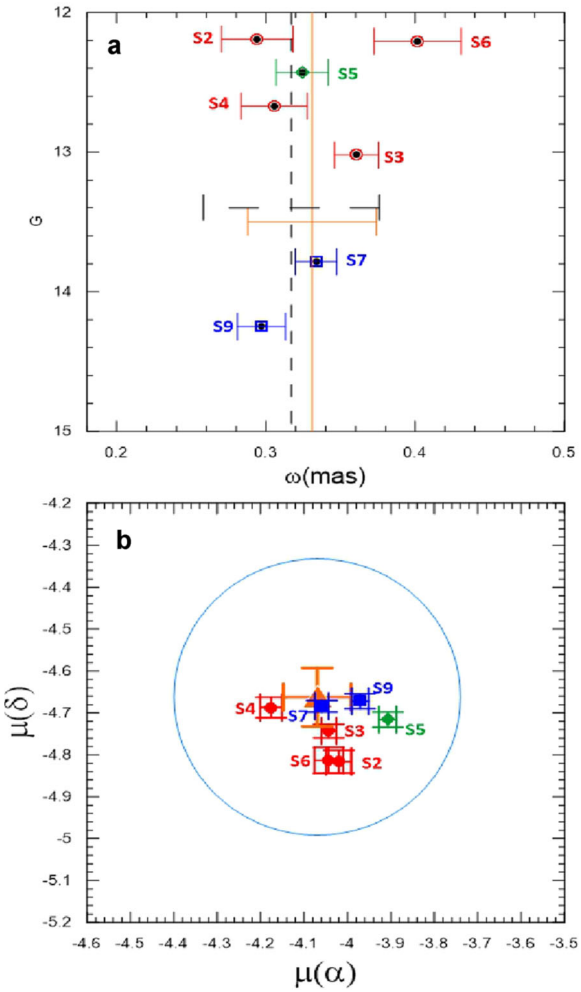

Figure 5. Gaia EDR3 parallax (ϖ) against G mag (panel a) and the μ_α *vs.* μ_δ (panel b) for five RSGs/RBGs and two BS candidates. The median Gaia EDR3/photometric parallaxes are shown with the vertical dashed black and solid orange lines together with their uncertainties (horizontal lines), respectively. The orange triangle of panel (b) denotes the median Gaia EDR3 proper motion components of Be 55. The blue circle represents the expected dispersion (0.33 mas yr^{-1}) in proper motion.

to calculate both the median values ($\langle\mu_\alpha\rangle$ and $\langle\mu_\delta\rangle$) and the quantity $\mu_{\rm R} = \sqrt{(\mu_\alpha - \langle\mu_\alpha\rangle)^2 + (\mu_\delta - \langle\mu_\delta\rangle)^2}$). A parallax histogram and a $(G, G_{\rm BP} - G_{\rm RP})$ diagram are presented in the bottom of Figure 4. The blue and black histograms show 305 and 109 members, respectively. One hundred and nine members are in good agreement with 107 members, classified by Cantat-Gaudin *et al.* (2018, 2020). The applied median Gaia EDR3 parallax ($\varpi = 0.317 \pm 0.059$ mas) on the histogram gives 64 members, and these provide a single stellar sequence (black dots) in the $(G, G_{\rm BP} - G_{\rm RP})$ diagram. Since the current Gaia EDR3 parallaxes of the individual stars have a random error, the ensemble median parallax is considered. Accordingly the parallax error is the median of the members. The median astrometric values of 64 members are $(\mu_\alpha, \mu_\delta) = (-4.070 \pm 0.078, -4.662 \pm 0.070)$ mas yr^{-1} and $\varpi = 0.317 \pm 0.059$ mas, respectively, which are compatible with $(\mu_\alpha, \mu_\delta) = (-4.050 \pm 0.219, -4.618 \pm 0.214)$ mas yr^{-1} and $\varpi = 0.309 \pm 0.091$ mas, given by Cantat-Gaudin *et al.* (2018, 2020).

The determination of the age of Be 55 depends on the memberships of five RSGs/RBGs and two BSs. As was done by Lohr *et al.* (2018) (see Figures 7–10), to

Table 5. Properties of seven bright stars in Be 55.

Star no. (N12/L18)	V (mag)	$(B-V)$	$(U-B)$	$E(J-K_S)/E(B-V)$	$m\,(M_\odot)$	M_V (mag)	ϖ (mas)	$d_{\rm Gaia}$ (kpc)	$d_{\rm ph.}$ (kpc)	SpT (A20)
S5/*L*107	14.106	2.340	1.582	0.863/1.726	5.9	−3.99	0.324 ± 0.017	3.09 ± 0.16	3.47 ± 0.45	F8Ib
S3/*L*163	14.754	2.588	1.866	0.933/1.866	5.8	−3.35	0.360 ± 0.015	2.78 ± 0.12	2.84 ± 0.37	G8II
S4/*L*110	14.437	2.604	1.840	0.885/1.770	5.9	−3.67	0.305 ± 0.022	3.28 ± 0.24	3.26 ± 0.42	K0Ib-II
S2/*L*196	14.094	2.796	1.826	1.006/2.012	6.0	−4.01	0.294 ± 0.024	3.40 ± 0.28	2.30 ± 0.30	K0Ib
S6/*L*145	14.266	2.825	1.628	0.906/1.812	6.0	−3.84	0.402 ± 0.029	2.49 ± 0.18	3.07 ± 0.40	K4II
S9/*L*198	15.186	1.562	0.524	–/1.770	7.5	−2.70	0.297 ± 0.016	3.37 ± 0.18	2.95 ± 0.38	B3-4IIIShell
S7/*L*94	14.666	1.543	0.581	–/1.770	7.5	−3.22	0.334 ± 0.014	2.99 ± 0.13	2.95 ± 0.38	B4IV

Note: N12: Negueruela & Marco (2012); L18: Lohr *et al.* (2018); A20: Alonso-Santiago *et al.* (2020).

query on their memberships further, their Gaia EDR3 parallaxes against G-mag plus μ_α *vs.* μ_δ are shown in Figures 5(a) and (b). In panel (a), the vertical lines indicate the median Gaia EDR3 parallax $\varpi = 0.317 \pm 0.059$ mas (dashed black line), and photometric parallax $\varpi = 0.331 \pm 0.043$ from $Q_{V\lambda} - Q'$ (orange line, see Section 3.4), respectively. As is noticed from panel (a), the parallax uncertainties of five RSGs/RBGs and two BSs (Table 5) almost remain within the error limits of the vertical/horizontal lines. Note that the *S6*/*L*145's parallax value is far from the median parallax. However, its uncertainty remains the error limit of the horizontal dashed line. Here, the notation "L" represents the star ID in Lohr *et al.* (2018) .

The proper motions of five RSGs/RBGs and two BSs together with their errors are inside the borders of the blue circle (panel b). A blue circle is constructed as the following, the derivation of the relation $V_{\rm tan} = 4.74\mu/\varpi$ provides $\sigma_{V(\rm tan)} = 4.74\sigma_\mu/\varpi$. In this case, it is assumed that the adopted ϖ has no error, and that the velocity of stars in Be 55 is homogeneous and isotropic, $\sigma_{V(\rm tan)} = \sigma_{V(\rm rad)}$. Alonso-Santiago *et al.* (2020) give the average radial velocity of the bright giants of Be 55 as $V_{\rm rad} = -27.7 \pm 4.9$ km s^{-1}. Then the expected dispersion in proper motion is obtained as $\sigma_\mu = (4.9\,{\rm km\,s^{-1}}) \times \varpi(= 0.317\,{\rm mas})/4.74 = 0.33$ mas yr^{-1}. In that case, these all seem to be members, for this respect, the derived age in this paper is safely interpreted. The global parallax zero-point shift, $\Delta\varpi = -0.017$ mas of Gaia EDR3 (Brown 2020) is applied to the median value, 0.317 mas, it gives a close distance up to 0.16 pc.

The distribution of 64 probable members on the CMDs, (*V*, *U*–*B*), (*V*, *B*–*V*), and (*V*, *V*–*I*) is shown in Figure 6. Maidanak UBVI CCD observations of the cluster on the CMDs are shown with grey symbols; 89 (panel a), 357 (panel b), and 403 (panel c), respectively.

3.3 *Reddening*

The reddening of Be 55 is determined from 38 early-type members with $V < 16$ mag and $(U-B) < 1.1$ on the $(U-B)$, $(B-V)$ colour–colour (CC) plot (Figure 7). Out of 64 members, 46 members have UBV data. Five members with a red circle are the RSGs/RBGs. The mean reddening from these early-type members is estimated as $E(B-V) = 1.77 \pm 0.10$ mag, and thus the reddened colour sequence of the Schmidt-Kaler (1982) (red curve) is fitted to the CC diagram. For the determination of $E(B-V)$, the reddenings $E(V-I)$, $E(V-J)$, $E(V-H)$, and $E(V-K_S)$ have been estimated by using the intrinsic colour relation of early-type stars, given by Sung *et al.* (2013) (see their Tables 2 and 3). Here the colour excess ratio $E(U-B) = 0.72E(B-V) + 0.025E\ (B-V)^2$ of Sung *et al.* (2013) is adopted. The reddening law of Be 55 using colour excess ratios $E(V-\lambda)$ for IJHK$_S$ photometry has been tested in Figure 8. Thirty-eight members (filled blue dots) lie on the solid line. The total-to-selective extinction ratio is obtained as $R_{\rm V} = 3.13 \pm 0.04$ (Table 6), which implies that the reddening law towards Be 55 is quite normal. According to Guetter & Vrba (1989), the colour excess ratio of optical–near infrared colours is related to the total-to-selective extinction ratio.

Its highly reddened value, $E(B-V) = 1.77 \pm 0.10$ mag is in agreement with $E(B-V) = 1.85$ mag of Negueruela & Marco (2012), $E(B-V) = 1.81 \pm 0.15$ mag of Alonso-Santiago *et al.* (2020), $E(B-V) = 1.75$ mag of Molina *et al.* (2018), $E(B-V) = 1.74$ mag of Lohr *et al.* (2018), and

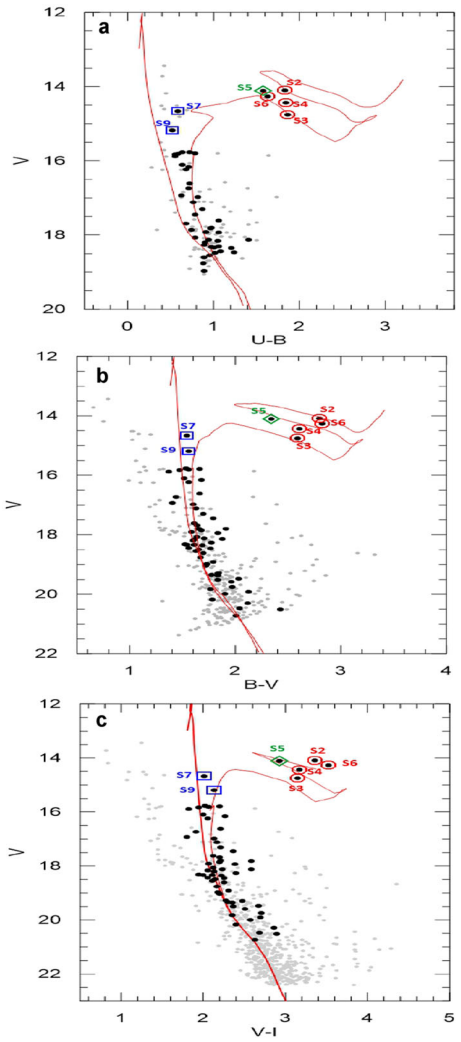

Figure 6. CMDs of the members; $V-(U-B)$ ($N=46$, panel a), $V-(B-V)$ ($N=64$, panel b) and $V-(V-I)$ ($N=64$, panel c). Solid red lines/curves denote the Ekström *et al.* (2012) ZAMS/85 Myr isochrones. Maidanak UBVI CCD observations are shown with grey symbols: 89 (panel a), 357 (panel b), and 403 (panel c), respectively. Diamond, filled red circles, and blue squares represent one Cepheid, four RSGs/RBGs, and two BSs, respectively. Star designation is from Negueruela & Marco (2012) .

$E(B-V) = 1.74 \pm 0.10$ mag of Maciejewksi & Niedzielski (2007) within the uncertainties (Table 1), respectively. This reddening is larger than the ones of Tadross (2008) and Bukowiecki *et al.* (2011). Note that Negueruela & Marco (2012) also give $E(J-K_S) = 0.85$ mag, which converts to $E(B-V) = 1.73$ mag *via* a relation $E(J-K_S) = 0.49E(B-V)$ of Dutra *et al.* (2002).

The reddening value derived from the early-type stars cannot be used to deredden late-type supergiants.

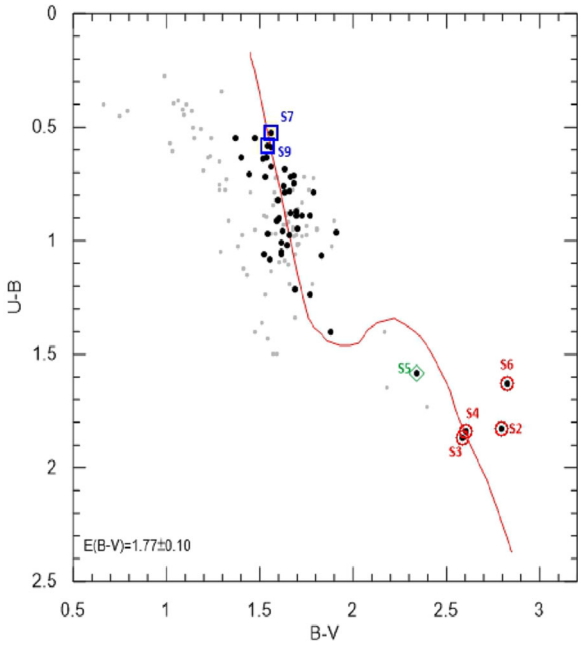

Figure 7. $(U-B)$, $(B-V)$ (CC) diagram for 38 members (filled dots) of Be 55. Grey symbols denote the 97 stars from Maidanak UBV CCD observations. The red curve shows the reddened Schmidt-Kaler (1982) main sequence. The symbols of bright evolved stars are the same as in Figure 6.

Therefore, the mean reddening value from their $(J-K_s)$ colours of the five evolved stars (Table 5) is estimated as $E(J-K_s) = 0.92 \pm 0.06$ mag, by utilising the intrinsic colour $(J-K_s)_0$ of Koornneef (1983). This converts to $E(B-V) = 1.84 \pm 0.11$ mag from the relation $E(J-K_s) = 0.49E(B-V)$ (Dutra *et al.* 2002). Their reddenings are listed in column 5 of Table 5. For Be 55, Alonso-Santiago *et al.* (2020) mention a non-negligible differential reddening. The reddened values $E(B-V) = 1.77 \pm 0.10$ mag (early-type stars) and $E(B-V) = 1.84 \pm 0.11$ mag (five evolved stars) imply a differential reddening in Be 55. The members selected in Figure 7 are scattered over >0.3 mag in $(B-V)$ for a given $(U-B)$. Similarly, the members are scattered over >0.5 mag in $(G, G_{BP}-G_{RP})$ (Figure 4).

The spatial variation of reddening of Be 55 as the reddening map is derived from its member stars (red dots) and field stars (black dots) and shown in Figure 9. The size of the dots is scaled to the magnitude of the star. The coloured line types as iso-reddening contours represent different amounts of reddening $E(B-V)$. From Figure 9, there seems to be a differential reddening across the cluster due to a slight variation of $E(B-V)$. Most young OCs with ages younger than 10 Myr show a differential

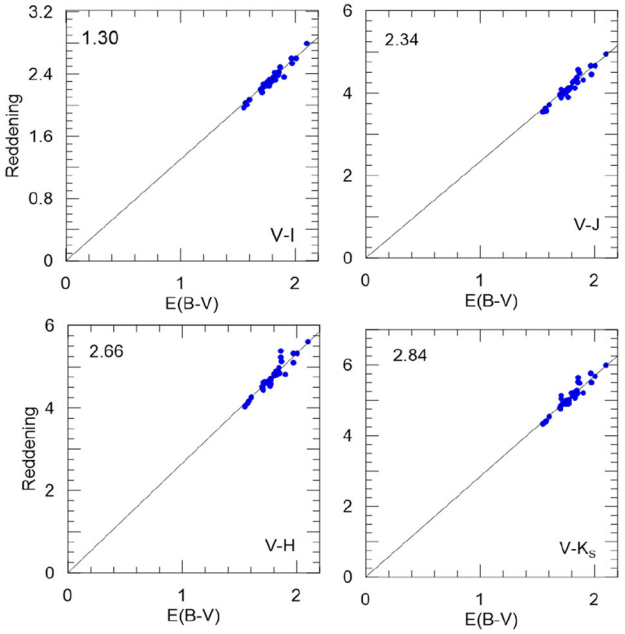

Figure 8. $E(V-\lambda)$ *vs.* $E(B-V)$ relations. λ denotes the IJHK$_S$ photometry. The solid line means $R_V = 3.1$. The colour excess ratios from the IJK$_S$ data consistently show that the reddening law towards Be 55 is normal

Table 6. $E(V-\lambda)/E(B-V)$ ratios in terms of four colour indices. R_V is the weighted average of four colours. Here λ is I, J, H and K$_s$. N (last column): cluster star numbers.

Colour	$E(V-\lambda)/E(B-V)$	N
V–I	1.300 ± 0.050	38
V–J	2.341 ± 0.131	38
V–H	2.659 ± 0.172	38
V–K$_s$	2.841 ± 0.177	38
$R_V = 3.13 \pm 0.04$		

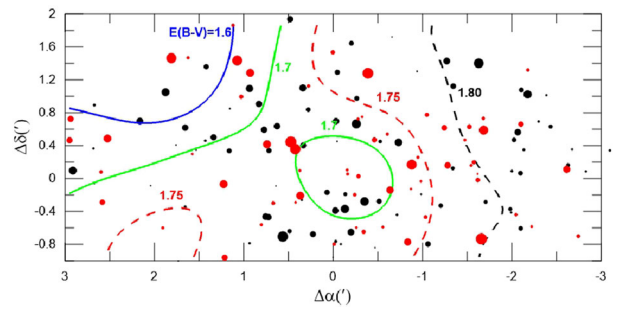

Figure 9. Reddening map of Be 55. Red and black dots show the member and field stars, respectively. The size of the dots is scaled to the magnitude of the star. The coloured line types as iso-reddening contours represent different amounts of reddening $E(B-V)$.

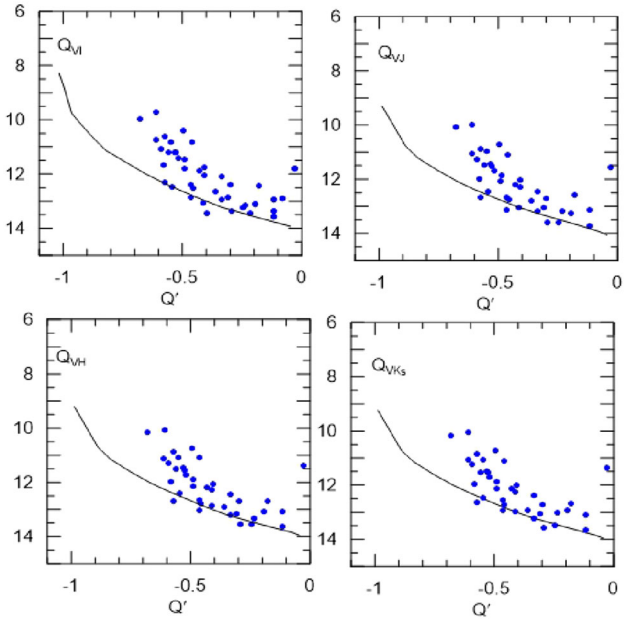

Figure 10. $Q_{V\lambda}$ *vs.* Q' diagrams (38 early-type members, filled blue dots) for determination of distance modulus of Be 55. λ denotes the IJHK$_S$ filters. A careful ZAMS fitting to the lower boundary of the MS band was carried out in the reddening-independent $Q_{V\lambda}$–Q' planes. The ZAMS relation of Sung *et al.* (2013) is used to determine the distance to the cluster after adjusting by 12.4 ± 0.2.

reddening across the field of view. However, for slightly old OCs, it is not well known whether there is a differential reddening across the cluster or not. That is the reason to check the differential reddening across the cluster.

3.4 *Distance*

Instead of the reddening-corrected CMDs, the distance modulus/distance of Be 55 is obtained by using the Zero Age Main Sequence (ZAMS) fitting method with the reddening-independent indices (Sung *et al.* 2013). For this, UBVRIJHK$_s$ photometry of 38 early-type stars is used. The reddening-independent quantities, Q', Q_{VI}, Q_{VJ}, Q_{VH} and Q_{VK_S}, are utilised. The $Q_{V\lambda}$–Q' plots for 38 early-type members have been shown in Figure 10. Solid lines denote the fitted ZAMS relation of Sung *et al.* (2013) to the members. As suggested by Lim *et al.* (2014), ZAMS should be fitted to the lower ridge of the main-sequence (MS) band to avoid the effects of multiplicity and evolution. The ZAMS line is shifted up and down in Figure 10 by 0.1 mag. The error of this method is about 0.20 mag.

Once the ZAMS has been adjusted above and below the distribution of the members (Figure 10), the distance modulus from four colour indices is obtained as $(V_0 - M_V) = 12.40 \pm 0.20$ mag, equivalent to 3.02 ± 0.28 kpc, which is adopted for this paper. The median Gaia EDR3 parallax is $\varpi = 0.317 \pm 0.059$ mas, which corresponds to $(V_0 - M_V) = 12.49 \pm 0.41$ mag ($d = 3.15 \pm 0.59$ kpc). The two distances are compatible with the uncertainties.

4. Age of Be 55

The $M_{\rm bol} - \log T_{\rm eff}$ diagram (HRD) for 46 members (41 early types and five RSGs/RBGs) is shown in Figure 11. Their effective temperature and BC values have been determined from their $(U-B)_0$ and $(B-V)_0$ by utilising Table 5 of Sung *et al.* (2013). Their $M_{\rm bol}$ values are obtained from the relation $M_{\rm bol} = {\rm BC} + V - R_V E(B-V) - (V_0 - M_V)$. For this, the UBV photometry of 41 early types and five RSGs/RBGs is de-reddened by $E(B-V) = 1.77$ mag and $E(B-V) = 1.84$ mag, respectively.

The metal abundance, $[M/H] = 0.07 \pm 0.12$ ($Z = 0.014$) of Be 55, given by Lohr *et al.* (2018) is considered for selecting the isochrone. Note that Be 55 has an extended main sequence. Due to the diversity of the rotational velocity even in a cluster (Lim *et al.* 2019), MS turn-off broadens. Broadening in the main sequence of the color-magnitude diagram (CMD) could be also due to the binarity, peculiarity, rotation in the stars. Therefore, the solar abundance Geneva models of Ekström *et al.* (2012) ($V/V_{\rm crit} = 0.4$) and Georgy *et al.* (2013) (for B-type stars and $V/V_{\rm crit} = 0.3$) have been fitted to the members in the $M_{\rm bol} - \log T_{\rm eff}$ (Figure 11) and de-reddened $(V_0, B-V_0)$ (Figure 12). $(V_0 - M_V) = 12.40 \pm 0.20$ mag (Q technique) and the reddenings $E(B-V) = 1.77 \pm 0.10$ mag (for early-type stars) and $E(B-V) = 1.84 \pm 0.11$ mag (for evolved stars) have been applied to the Ekström *et al.* (2012) and Georgy *et al.* (2013) isochrones while fitting.

As is seen in Figure 11, the 85 ± 13 Myr Ekström *et al.* (2012) isochrone with high rotation (blue curve) describes the general morphology of Hertzsprung Russell Diagram (HRD) without accurate locations. The 85 Myr Ekström *et al.* (2012) isochrone (blue curve) is almost consistent with the RSGs/RBGs, *S*4/*L*110, *S*5/*L*107 (Cepheid), and *S*6/*L*145, except for *S*3/*L*163. Also, the 70±10 Myr Georgy *et al.* (2013) isochrone (red curve) with a moderate rotation for B-type stars provides a good fit with the RSGs/RBGs, *S*2/*L*196, *S*4/*L*110 and *S*5/*L*107 (Cepheid), except for *S*3/*L*163 and *S*6/*L*145. Note that *S*5/*L*107 appears to be on the core-He burning blue loop. Note that non-rotating Ekström *et al.* (2012) isochrone (blue dashed line) gives a faint turn-off, and going below the RSGs/RBGs.

On the $V_0 - (B-V)_0$ (Figure 12), *S*2/*L*196 and three RSGs/RBGs occupy positions that are consistent with the 85 Myr Ekström *et al.* (2012) isochrone. However, the 70 Myr Georgy *et al.* (2013) isochrone is not compatible with the positions of the RSGs/RBGs.

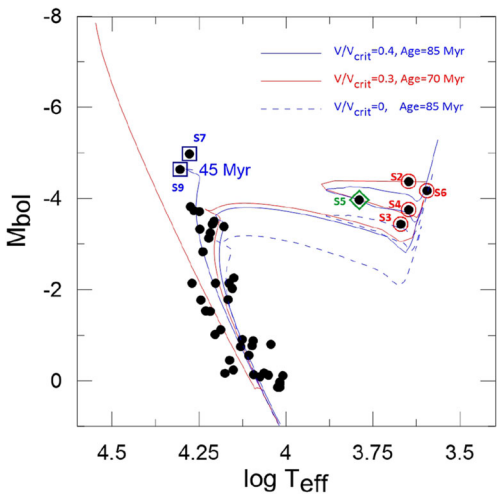

Figure 11. $M_{\rm bol}$ *vs.* $\log T_{\rm eff}$ of 46 probable members. Solid and dashed blue curves represent rotating/non-rotating Ekström *et al.* (2012) isochrones. Red curve shows Georgy *et al.* (2013) isochrone for B-type stars with $V/V_{\rm crit} = 0.3$. The solid red line represents the ZAMS of Ekström *et al.* (2012). The symbols are the same as in Figure 6.

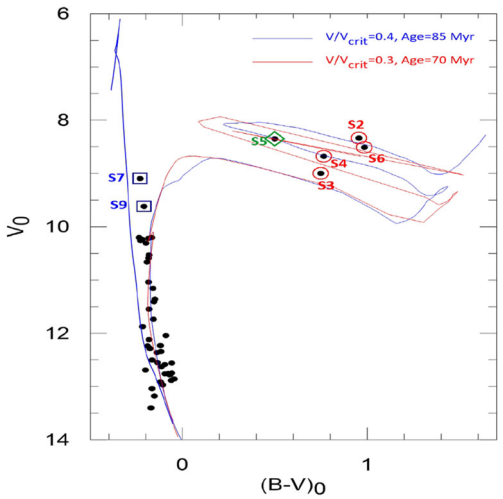

Figure 12. $V_0 - (B-V)_0$ of 46 probable members. The symbols are the same as in Figure 11.

The two BSs, *S*9/*L*198 and *S*7/*L*94, are located between ZAMS and the 45 Myr isochrone (Figures 11 and 12). The age of BSs seems to be definitely younger than the cluster. From Figures 11 and 12, there appears an extended MS turn-off, since the main sequence band is expected to broaden in CMDs due to their different main sequence lifetimes. Also, the broadening in the MS band may also be due to differential reddening across the cluster because the scatter in $E(B-V)$ is about 0.1 mag (Section 3.3). One can expect about 0.3 mag scatter (3σ). since the width of the MS band is about 0.3 mag.

5. Kinematics and orbital parameters

From the radial velocities of Alonso-Santiago *et al.* (2020) and the Gaia EDR3 proper motions for five RSGs/RBGs, their heliocentric velocities (U, V, W) in the right-hand system have been calculated from the algorithm of Johnson & Soderblom (1987). The photometric distance of Be 55 (3.02 ± 0.28 kpc) is adopted instead of their individual parallaxes. These space velocities are transformed to the components U', V', W' by correcting for the solar motion $(U,V,W)_{\odot} = (+11.10, +12.24, +7.25)$ km s^{-1} with respect to the local standard of rest (LSR) (Schönrich *et al.* 2010). Here, $R_{\odot} = 8.2 \pm 0.1$ kpc (Bland-Hawthorn & Ortwin 2016) and $V_{\rm LSR} = 239$ km s^{-1} (Brunthaler *et al.* 2011) are adopted. The heliocentric Cartesian distances (x', y', z') (kpc) and (Local Standard of Rest) LSR-velocity components (U', V', W') have been transformed to Galactic Standard of Rest (GSR), i.e., (x, y, z) (kpc) and (V_x, V_y, V_z) from the equations of Kepley *et al.* (2007). The galactocentric velocity component (V_{Φ}) (km s^{-1}) (or azimuthal velocity) in a cylindrical frame is estimated *via* $V_{\Phi} = xV_y - yV_x/R$. Here, $V_{\Phi} < 0$ means prograde. By utilising the "MWPotential2014" code in the galpy-code library[1] written by Bovy (2015), peri- and apo-galactic distances ($R_{\rm min}, R_{\rm max}$) (kpc) and the maximum height distance ($z_{\rm max}$) (kpc) have been obtained. The orbital eccentricity (ecc) is estimated *via* the relation $e = (R_{\rm max} - R_{\rm min})/(R_{\rm max} + R_{\rm min})$. Five evolved member's orbits have been integrated for 85 Myr within the galactic potential. The galactic potential as the sum of the galactic components is explained by Bovy (2015). Their orbital angular momentum components J_x, J_y, J_z and $J_{\perp}$ (kpc km s^{-1}) are calculated from the equations of Kepley *et al.* (2007). The total angular momentum J$_{\perp}$ is defined as $J_{\perp} = (J_x^2 + J_y^2)^{1/2}$. The relations of x–y (kpc) and z- R (kpc) of the five RSGs/RBGs are shown in Figure 13.

[1] http://github.com/jobovy/galpy.

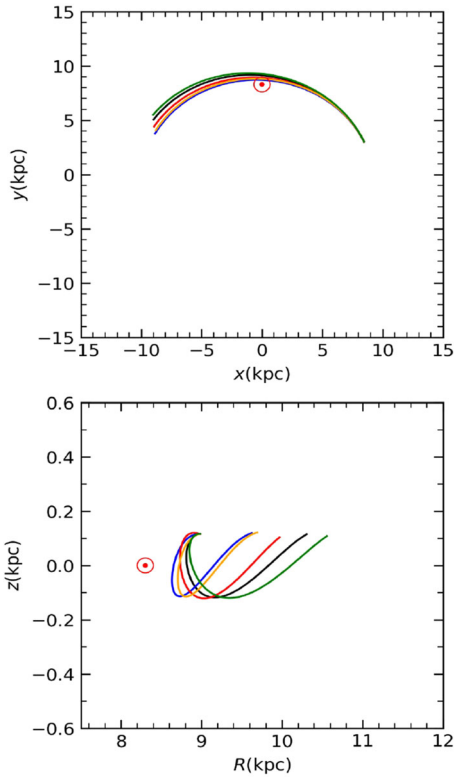

Figure 13. Orbits of five RSGs/RBGs on x–y (kpc) (top panel) and z–R (kpc) (bottom panel). A large circle shows the position of the Sun, $(z_{\odot}, R_{\odot}) = (0, 8.2\,{\rm kpc})$.

6. Discussion and conclusion

The photometric distance modulus/distance of Be 55 as $(V_0 - M_V) = 12.40 \pm 0.20$ mag (3.02 ± 0.28 kpc) is better and consistent with the median Gaia EDR3 distance (3.15 ± 0.59 kpc). These distances locate Be 55 near the Perseus spiral arm. The photometric distance of this paper is in concordance with 3.24 ± 0.22 kpc of Alonso-Santiago *et al.* (2020) and 3.02 kpc of Molina *et al.* (2018) (Table 1). It is rather smaller than Negueruela & Marco (2012) but is farther than Lohr *et al.* (2018) . Lohr *et al.* (2018) distance is from the period–luminosity relation (PLR) of Cepheid *S*5 (Table 7). Negueruela & Marco (2012) obtain its distance modulus from the dereddened ZAMS of Mermilliod (1981) and Schmidt-Kaler (1982) as 13.0 $\pm$ 0.30 mag on $M_V - (B-V)$. This corresponds to a distance of 3.98 $\pm$ 0.55 kpc. Lohr *et al.* (2018) distance locates Be 55 on the outer edge of the local arm

Table 7. Distances for the values of V, M_V, $P = 5.85$ days, and $E(B-V)$ of Cepheid *S*5. The methods and their references for M_V are listed in columns 5 and 6.

d (kpc)	V (mag)	M_V (mag)	$E(B-V)$ (mag)	Methods for M_V	References	Remarks
3.47 ± 0.45	14.106	−3.99	1.73	Ekström *et al.* (2012) isochrone	Akkaya *et al.* (2019)	This paper
2.78 ± 0.32	14.106	−3.52	1.73	$-(2.67 \pm 0.16)(\log P - 1) - (4.14 \pm 0.05)$	Akkaya Oralhan *et al.* (2020)	This paper
3.09 ± 0.16	–	–	–	–	–	Gaia EDR3
2.20 ± 0.30	13.834	−3.23	1.74	$-(2.88 \pm 0.18)\log P - (1.02 \pm 0.16)$	Alonso-Santiago *et al.* (2017)	L18
2.40 ± 0.30	13.834	−3.93	1.74	$-(2.43 \pm 0.12)(\log P - 1) - (4.5 \pm 0.02)$	Alonso-Santiago *et al.* (2020)	L18
3.03 ± 0.37	13.834	–	1.81	$a(\log P - 1) + b$, for JHK	Anderson *et al.* (2013)	A20

L18: Lohr *et al.* (2018); A20: Alonso-Santiago *et al.* (2020).

Table 8. Available Gaia EDR3 proper motion components (mas yr^{-1}) and spectroscopic radial velocity data (km s^{-1}) of five RSGs/RBGs, kinematics (U, V, W, V_Φ) km s^{-1}, orbital parameters (R_{max}, R_{min}, z_{max}) (kpc), eccentricity (ecc), and angular momentums (J_z and $J_\perp$) (kpc km s^{-1}), respectively

Star	μ_α	μ_δ	V_{rad}	
S2	-4.020 ± 0.029	-4.816 ± 0.027	-24.55 ± 0.39	
S3	-4.043 ± 0.017	-4.743 ± 0.016	-33.33 ± 0.47	
S4	-4.176 ± 0.025	-4.687 ± 0.024	-28.97 ± 0.47	
S5	-3.907 ± 0.020	-4.716 ± 0.018	-31.63 ± 0.86	
S6	-4.043 ± 0.033	-4.813 ± 0.031	-21.61 ± 0.60	
	U	V	W	V_Φ
S2	90.71	−19.59	−7.55	−252.38
S3	90.66	−28.39	−6.88	−244.08
S4	91.18	−24.04	−4.84	−248.35
S5	88.94	−26.72	−7.97	−245.07
S6	90.76	−16.60	−7.23	−255.22
	R_{min}	R_{max}	ecc	
S2	8.81	10.31	0.08	
S3	8.63	9.62	0.05	
S4	8.73	9.97	0.07	
S5	8.70	9.69	0.05	
S6	8.85	10.56	0.09	
	z_{max}	J_z	$J_\perp$	
S2	0.12	−2266	24	
S3	0.12	−2192	24	
S4	0.12	−2230	33	
S5	0.12	−2200	24	
S6	0.13	−2292	24	

rather than in the Perseus arm as Negueruela & Marco (2012) suggest. A mismatch between the distances of Lohr *et al.* (2018) and Negueruela & Marco (2012) is explained by the underestimated uncertainties in Negueruela & Marco (2012) distance modulus. The other literature gives close distances.

The distance, 2.78 kpc, of Cepheid *S5*/*L*107 from the PLR of Lazovik & Rastorguev (2020) is consistent with the ones of Gaia EDR3 and Alonso-Santiago *et al.* (2020) within the errors (Table 8). Note that Lohr *et al.* (2018) give close distances. $M_V = -3.99$ from Ekström *et al.* (2012) isochrone estimates a large distance of 3.47 kpc.

The Ekström *et al.* (2012) isochrone (high rotation) fittings to HRD/CMD derive turn-off age, 85 ± 13 Myr of Be 55, by taking care of five RSGs/RBGs. For this age, the masses of five RSGs/RBGs from the Ekström *et al.* (2012) isochrone are about 6 $M_\odot$ (column 6 of Table 5). The 70 Myr Georgy *et al.* (2013) isochrone with a moderate rotation does not provide a good fit to the RSGs/RBGs on the $V_0 - (B-V)_0$ (Figure 12). The age 85 Myr is somewhat older than Negueruela & Marco (2012), Lohr *et al.* (2018), and Alonso-Santiago *et al.* (2020) (Table 1) but falls in the range of 30–100 Myr of Molina *et al.* (2018). From the non-rotating PARSEC isochrones, Alonso-Santiago *et al.* (2020) give its age as 63 ± 15 Myr (see their Figure 6 and Table 1), by considering evolved members. The age 85 Myr also falls in the range of 63–105 Myr, which is found from the period–age relations in Table 14 of Alonso-Santiago *et al.* (2020) for Cepheid *S5*/#107. Note that Negueruela & Marco (2012) apply two isochrones of Marigo *et al.* (2008); $\log t = 7.6$ (40 Myr) and $\log t = 7.7$ (50 Myr) on $(V, U-B)$. By taking $E(J-K_S) = 0.85$ mag, Negueruela & Marco (2012) also apply the same isochrones to $(K_S, J-K_S)$, and give an age of 50 Myr. The other literature values find more old ages (Table 1) than this paper.

From Table 1, note that Cantat-Gaudin *et al.* (2018, 2020) from Gaia DR2 photometry give a less reddening, a close distance, and an old age of 200 Myr, as compared with the values of this paper.

The spread of the brightness of the RSGs/RBGs in the HRD/CMDs indicates a much large spread in age. This feature may be the result of the diversity of stellar rotation among evolved cluster members (Sung *et al*. 1997; Lim *et al*. 2016, 2019), which indicates the necessity of cluster isochrone with a non-single rotational velocity distribution. The stars in OCs do not have the same rotational velocity (Lim *et al.* 2019). Some stars have very low rotational velocities, and some may be fast rotators. For that case, even the same mass stars are not in the same position in the HRD because fast rotators have a longer MS lifetime. This feature also indicates the necessity of cluster isochrones with a non-single rotational velocity distribution. As a result, the possible inconsistency in the locations of the RSGs/RBGs to the rotating/non-rotating isochrones may be resulting from the age spread of stars in young OCs. According to Alonso-Santiago *et al.* (2020), the possible inconsistence of the locations of the RSGs/RBGs on HRD/CMD is due to the strong reddening, rather than metal abundance.

Two BS candidates in $V_0 - (B-V)_0$ (Figure 12) lie on $(V_0 < 10.01\,\text{mag})$ $(V < 15.50$ mag) and $((B-V)_0 < 0.03)$ $(B-V) < 1.80$. These limits for V_0 and $(B-V)_0$, which BSs occupy in CMDs are similar to those given by [Carney (2001), Figure 19] and [Carraro *et al.* (2010), Figure 10]. The positions of two BSs are located between ZAMS and the 85 Myr isochrone. The age of BSs is definitely younger than the cluster. Therefore, the 45 Myr isochrone is drawn up to MS turn-off. As discussed by Ferraro (2016), BSs are commonly defined as stars brighter and bluer than the MS turnoff in open/globular clusters. Therefore, their origin cannot be explained with a normal single star evolution. Two main formation mechanisms are proposed: (1) mass transfer in the binary systems (McCrea 1964) possibly up to the complete coalescence of the two stars and (2) stellar collisions (Hills & Day 1976). Both these processes can potentially bring a new hydrogen into the core and therefore "rejuvenate" a star to its MS stage (Lombardi *et al.* 2002; Chen & Han 2009). According to Sandage (1953) and Tout *et al.* (1997), the increase in mass of a star makes it look younger than it is.

The kinematics, orbital, and angular momentum values of the five evolved members (Table 8) indicate that Be 55 is a member of the galactic thin disk population, which is also consistent with its metallicity, $[M/H] = 0.07 \pm 0.12$. With circular orbits, ecc $= [0.05, 0.09]$, Be 55 does not seem to have completed a tour around the center of the Galaxy (top panel of Figure 13). They reach $z \sim 0.13$ kpc and their birthplaces are at ~ 9 kpc (bottom panel of Figure 13). However, their orbits show that the cluster passed a part of its time at $R_{\min} = 8.63 - 8.85$ kpc.

The total mass for 64 early-type members is obtained as $M_{\text{tot}} = 224\,M_\odot$ from 85 Myr Ekström *et al.* (2012) isochrone. From the photometric distance (3.02 ± 0.28 kpc) and angular size $\theta \sim 0.073°$ (0.0013 in rad), the diameter of Be 55 is determined as 3.85 pc. To check its stability, the maximum tangential velocity of the members within the radius of $\mu = 0.5$ mas yr^{-1} is estimated as 7.2 km s^{-1}, *via* the relation, $V_{\tan} = 4.74\mu \times d\,(\text{kpc})$. These values indicate that its virial mass is about $M_{\text{vir}} = 25,100\,M_\odot$, which is far larger than the cluster mass, 224 $M_\odot$.

Be 55 with its total mass, 224 $M_{\odot}$, depending on its location of $R_{GC} = 9.04$ kpc and $\ell = 93°.03$ is a survivor against internal and external perturbations related to, for example, stellar evolution, mass segregation, spiral arms, and encounters with the disk and giant molecular clouds.

Acknowledgements

The author thanks H. Sung for providing his private photometric data and the interpretations on the analysis. Y. Karatas and H. Cakmak are also thanked for the kinematics and dynamics. The referee is thanked for the useful suggestions. This paper has made use of results from the European Space Agency (ESA) space mission Gaia, the data from which were processed by the Gaia Data Processing and Analysis Consortium (DPAC). Funding for the DPAC has been provided by national institutions, in particular, the institutions participating in the Gaia Multilateral Agreement. The Gaia mission website is http://www.cosmos.esa.int/gaia.

References

Akkaya Oralhan Í., Michel R., Schuster W. J., *et al.* 2019, J. Astrophys. Astron., 40, 33
Akkaya Oralhan, Í., Michel R., Karslı Y., *et al.* 2020, Astron. Nach., 341, 44
Alonso-Santiago J., Negueruela I., Marco A., *et al.* 2017, Mon. Not. R. Astron. Soc., 469, 1330
Alonso-Santiago J., Negueruela I., Marco A., *et al.* 2020, 2009.124118v, Astron. Astrophys., 644A, 136
Anderson R. I., Eyer L., Mowlavi N. 2013, Mon. Not. R. Astron. Soc., 434, 2238
Arellano Ferro A., Giridhar S., Rojo Arellano E. 2003, RevMexAA, 39, 3
Benedict G. F., *et al.* 2007, Astron. J., 133, 1810
Bertelli G., Bressan A., Chiosi C., *et al.* 1994, Astron. Astrophys. Suppl. Ser., 106, 275
Bland-Hawthorn J., Ortwin Gerhard O. 2016, Annu. Rev. Astron. Astrophys., 54, 529
Bonatto Ch., Bica E., Girardi L. 2004, Astron. Astrophys., 415, 571
Bonatto Ch., Bica E. 2007, Astron. Astrophys., 473, 445
Bovy J. 2015, Astrophys. J. Suppl., 216, 29
Bressan A., Marigo P., Girardi L., *et al.* 2012, Mon. Not. R. Astron. Soc., 427, 127
Brown A. G. A., Vallenari A., Prusti T., *et al.* 2018, Astron. Astrophys., 616, 1G
Brown A. G. A., Vallenari A., Prusti T., *et al.* 2020, 2020arXiv201201533G
Brunthaler A., Reid M. J., Menten K. M., *et al.* 2011, Astron. Nachr., 332, 461
Bukowiecki L., Maciejewski G., Konorski P., *et al.* 2011, Acta Astron. 61, 231
Cantat-Gaudin T., Jordi C., Vallenari A., *et al.* 2018, Astron. Astrophys., 618, 93
Cantat-Gaudin T., Anders F., Castro-Ginard A., *et al.* 2020, Astron. Astrophys., 640, 1
Carney B. 2001, in Labhardt L., Binggeli B. (eds). Star Clusters, Saas-Fee Advanced Course 28, Lecture Notes 1998, Swiss Society for Astrophysics and Astronomy. Berlin, Springer-Verlag, p. 1
Carraro G., Costa E., Ahumada J. A. 2010, Astron. J., 140, 954
Chen X. F., Han Z. W. 2009, Mon. Not. R. Astron. Soc., 395, 1822
Chen X., de Grijs R., Deng L. 2017, Mon. Not. R. Astron. Soc., 464, 119
Chiosi C., Bertelli G., Bressan A. 1992, Annu. Rev. Astron. Astrophys., 30, 235
Dutra C. M., Santiago B. X., Bica E. 2002, Astron. Astrophys., 383, 219
Ekström S., Georgy C., Eggenberger P., *et al.* 2012, Astron. Astrophys., 537, 146
Fernie J. D. 1963, Astron. J., 68, 780
Ferraro F. R. 2016, Star clusters and black holes in galaxies across cosmic time. In Proceedings of the International Astronomical Union, IAU Symposium, volume 312, p. 171
Fiorentino G., Lanzoni B., Dalessandro E., *et al.* 2014, Astrophys. J., 783, 34
Fitzgerald M. P. 1970, Astron. Astrophys., 4, 234
Gilliland R. L., Bono,G., Edmonds P. D., *et al.* 1998, Astrophys. J., 507, 818
Girardi L., Bertelli G., Bressan A., *et al.* 2002, Astron. Astrophys., 391, 195
Georgy C., Ekström S., Granada A., *et al.* 2013, Astron. Astrophys., 553, 24
Guetter H. H., Vrba F. J. 1989, Astron. J., 98, 611
Hills J., Day C. 1976, Astron. Lett., 17, 87
Johnson D. R. H., Soderblom D. R. 1987, Astron. J., 93, 864
Kepley A., Morrison H. L., Helmi A., *et al.* 2007, Astron. J., 134, 1579
Kharchenko N. V., Piskunov A. E., Schilbach E., *et al.* 2013, Astron. Astrophys., 558, 53
Kilkenny D., Van Wyk F., Roberts G., *et al.* 1998, Mon. Not. R. Astron. Soc., 294, 93
King I. 1966, Astron. J., 71, 64
Koornneef J. 1983, Astron. Astrophys., 128, 84
Lazovik Y. A., Rastorguev A. S. 2020, Astron. J., 160, 2020
Li C., de Grijs R., Deng L., *et al.* 2017, Astrophys. J., 844, 119
Lim B., Sung H., Bessell M. S., *et al.* 2009, J. Korean Astron. Soc., 41, 161
Lim B., Sung H., Kim J. S., *et al.* 2014, Mon. Not. R. Astron. Soc., 443, 454

Lim B., Sung H., Kim J. S., *et al.* 2016, Astrophys. J., 831, 116
Lim B., Rauw G., Nazé Y., *et al.* 2019, NatAs, 3, 76
Lindegren L., Hernandez J., Bombrun A., *et al.* 2018, Astron. Astrophys., 616, A2
Lindegren L., Hernandez J., Bombrun A., *et al.* 2020, 2020arXiv201201533G
Lohr M. E., Negueruela I., Tabernero H. M., *et al.* 2018, Mon. Not. R. Astron. Soc., 478, 3825
Lombardi Jr. J. C., Warren J. S., Rasio F. A., *et al.* 2002, Astrophys. J., 568, 939
Maciejewski G., Niedzielski A. 2007, Astron. Astrophys., 467, 1065
McCrea W. H. 1964, Mon. Not. R. Astron. Soc., 128, 147
Marco A., Negueruela I., Gonzalez-Fernandez C., *et al.* 2014, Astron. Astrophys., 567, 73
Marigo P., Girardi L., Bressan A., *et al.* 2008, Astron. Astrophys., 482, 883
Mermilliod J.-C. 1981, Astron. Astrophys., 97, 235
Menzies J. W., Marang F., Laing J. D., *et al.* 1991, Mon. Not. R. Astron. Soc., 248, 642
Molina Lera J. A., Baume G., Gamen R. 2018, Mon. Not. R. Astron. Soc., 480, 2386
Negueruela I., Marco A. 2012, Astron. J., 143, 46
Negueruela I., Clark J. S., Dorda R., *et al.* 2016, in Skillen I., Balcells M., Trager S. (eds). ASP Conference Series, San Francisco, Astronomical Society of the Pacific (ASPC), volume 507, p. 75
Negueruela I., Monguio M., Marco A., *et al.* 2018, Mon. Not. R. Astron. Soc., 477, 2976
Sampedro L., Dias W. S., Alfaro E. J., *et al.* 2017, Mon. Not. R. Astron. Soc., 470, 3937
Sandage A. R. 1953, Astron. J., 58, 61
Schmidt-Kaler Th. 1982, in Schaifers K., Voigt H. H. (eds) Landolt-Bornstein: Numerical Data and Functional Relationships in Science and Technology, New Series, Group VI, Volume 2b, Berlin, Springer, p. 14
Schönrich R., Binney J., Dehnen W. 2010, Mon. Not. R. Astron. Soc., 403, 1829
Sung H., Bessell M. S. 1999, Mon. Not. R. Astron. Soc., 306, 361
Sung H., Bessell M. S., See-Woo L. 1997, Astron. J., 114, 2644
Sung H., Lim B., Bessell M. S., *et al.* 2013, J. Korean Astron. Soc., 46, 97
Tadross A. L. 2008, Mon. Not. R. Astron. Soc., 389, 285
Tout C. A., Aarseth S. J., Pols O. R., *et al.* 1997, Mon. Not. R. Astron. Soc., 291, 732